Applied Catalysis B: Environmental 144 (2014) 730–738

Contents lists available at ScienceDirect

Applied Catalysis B: Environmental

journal homepage: www.elsevier.com/locate/apcatb

One-step hydrothermal synthesis of high-performance visible-light-driven SnS_2/SnO_2 nanoheterojunction photocatalyst for the reduction of aqueous Cr(VI)

Yong Cai Zhang[a,b,*], Long Yao[a], Geshan Zhang[b], Dionysios D. Dionysiou[b,c,**], Jing Li[d], Xihua Du[d]

[a] Key Laboratory of Environmental Material and Environmental Engineering of Jiangsu Province, School of Chemistry and Chemical Engineering, Yangzhou University, Yangzhou 225002, China
[b] Environmental Engineering and Science Program, 705 Engineering Research Center, University of Cincinnati, Cincinnati, OH 45221-0012, USA
[c] Nireas-International Water Research Centre, University of Cyprus, 20537 Nicosia, Cyprus
[d] School of Chemistry and Chemical Engineering, Xuzhou Institute of Technology, Xuzhou 221111, China

ARTICLE INFO

Article history:
Received 14 June 2013
Received in revised form 29 July 2013
Accepted 6 August 2013
Available online 19 August 2013

Keywords:
SnS_2/SnO_2 nanoheterojunctions
One-step hydrothermal synthesis
Photocatalysis
Cr(VI) reduction

ABSTRACT

A simple and cost-effective one-step hydrothermal method, which was based on the reactions of tin(IV) chloride pentahydrate and different dosages of thioacetamide in water at 190 °C for 6 h, was employed for the synthesis of composition-tunable SnS_2/SnO_2 nanoheterojunctions (e.g., SnS_2/SnO_2-A, SnS_2/SnO_2-B and SnS_2/SnO_2-C). The photocatalytic properties of the as-synthesized SnS_2/SnO_2 nanoheterojunctions were tested by the reduction of aqueous Cr(VI) under visible-light ($\lambda > 420$ nm) irradiation. Furthermore, the photocatalytic efficiency of SnS_2/SnO_2-B was compared with those of PM-SnS_2/SnO_2 (which denotes the physically mixed SnS_2/SnO_2 nanocomposite with the same composition as SnS_2/SnO_2-B) and SnS_2 nanoflakes at different dosages of photocatalysts. It was observed that (i) the photocatalytic activities of the as-synthesized SnS_2/SnO_2 nanoheterojunctions depended on their compositions, and SnS_2/SnO_2-B with 70 mol% SnS_2 displayed the highest photocatalytic activity; (ii) SnS_2/SnO_2-B invariably exhibited higher photocatalytic efficiencies than PM-SnS_2/SnO_2 and SnS_2 nanoflakes at different dosages of photocatalysts; (iii) the washing with 1 mol/L HNO_3 can effectively regenerate the used photocatalyst; (iv) SnS_2/SnO_2-B exhibited good photocatalytic stability in reuses, with regeneration by 1 mol/L HNO_3-washing after each cycle of photocatalytic use; and (v) Cr(VI) was reduced to Cr(III). The possible formation mechanism of SnS_2/SnO_2 nanoheterojunctions and the reasons accounting for the photocatalytic results were also discussed.

1. Introduction

Cr(VI) is a common pollutant in the effluents from electroplating, pigments and chromate industries [1–11]. It has high toxicity and high mobility in water, and can cause great harm to the environment, ecology and human health [1–11]. Therefore, how to economically, effectively and environmental-friendly abate aqueous Cr(VI) has aroused increasing concern [1–11]. Semiconductor-mediated photocatalytic reduction is a promising way of abating aqueous Cr(VI) [1–24], by virtue of its outstanding features such as (i) low cost, (ii) direct use of "free", infinite, clean and safe solar energy, (iii) no use and no release of other undesirable chemicals, and (iv) reusability. The reduced product is usually Cr(III), which is much less toxic than Cr(VI) and can be easily precipitated in neutral and alkaline solutions ($K_{sp}^{\ominus}(Cr(OH)_3) = 6.3 \times 10^{-31}$) and tackled as a solid waste [5]. However, at present, the lack of high-performance visible-light-driven photocatalysts obstructs the practical application of photocatalysis technology to large-scale Cr(VI) wastewater treatment. Hence, it is obliged to explore new photocatalysts with high photocatalytic activity and good stability in the reduction of aqueous Cr(VI) under visible-light, which constitutes ~46% of solar energy [5].

The construction of semiconductor heterojunctions has been proved to be a successful strategy for developing more efficient photocatalysts than single semiconductor [24–58]. The improved photocatalytic efficiency of semiconductor heterojunctions can be

* Corresponding author at: Key Laboratory of Environmental Material and Environmental Engineering of Jiangsu Province, School of Chemistry and Chemical Engineering, Yangzhou University, Yangzhou 225002, China.
Tel.: +86 51487962581; fax: +86 51487975244.
** Corresponding author at: Environmental Engineering and Science Program, 705 Engineering Research Center, University of Cincinnati, Cincinnati, OH 45221-0012, USA.
E-mail addresses: zhangyc@yzu.edu.cn (Y.C. Zhang), dionysios.d.dionysiou@uc.edu (D.D. Dionysiou).

0926-3373/$ – see front matter © 2013 Elsevier B.V. All rights reserved.
http://dx.doi.org/10.1016/j.apcatb.2013.08.006

largely ascribed to the enhanced separation of photogenerated electrons and holes through interfacial charge transfer [24–58]. Thus, the heterointerface between different semiconductors of composite photocatalysts, which serves as the channel of charge transfer, is of crucial importance. Nonetheless, the heterointerface between different semiconductors of composite photocatalysts can be manipulated by adjusting the synthesis methods and synthesis conditions [24–58].

Composite photocatalysts were conventionally prepared by physical mixing of different semiconductors. Unfortunately, the particles of the physically mixed different semiconductors are hard to contact each other tightly, so they are liable to separate and self-agglomerate when suspended in the aqueous solution. The heterointerface arises only when the particles of different semiconductors collide. Therefore, the charge transfer and separation in the physically mixed composite photocatalysts cannot be effectively promoted. By contrast, in situ chemical solution methods enable to prepare composite photocatalysts with more uniform mixing, more intimate contact and even stronger interaction between different components, which can provide the tight and firm heterointerface for charge transfer and reduce the separation and self-agglomeration of different components during photocatalytic use [24–30]. Consequently, the composite photocatalysts prepared via in situ chemical solution methods often exhibited higher photocatalytic efficiencies than those prepared by physical mixing methods [24–30]. Besides, one-step in situ chemical solution methods are generally simpler (e.g., less synthesis and washing procedures), less polluting (e.g., less synthesis and washing procedures need less water or other solvents, producing less wastes), less time-consuming, more efficient and more cost-effective in preparing heterojunction photocatalysts [24,25], as compared with multi-step ones.

SnS_2, an inexpensive and nontoxic semiconductor with a bandgap of 2.0–2.25 eV [59–62], has recently been proved to be a relatively stable and efficient visible-light-driven photocatalyst [59–62]. SnO_2 is a stable wide bandgap semiconductor (E_g = 3.56–3.66 eV [29–31]), and can form heterojunction with SnS_2 because of their matched band potentials [29]. In the very limited studies undertaken hitherto [29–31], SnS_2/SnO_2 composites have demonstrated great potential in achieving higher visible-light-driven photocatalytic activity than SnS_2. However, in these studies [29–31], SnS_2/SnO_2 composite photocatalysts were exploited for the degradation of organic dyes, rather than the reduction of Cr(VI). Moreover, the existing synthesis methods of SnS_2/SnO_2 composite photocatalysts involved multi-steps or toxic and expensive organic solvents [29–31].

Herein, a simple and cost-effective one-step hydrothermal method, which was based on the reactions of tin(IV) chloride pentahydrate and different dosages of thioacetamide in water at 190 °C for 6 h, was employed for the synthesis of composition-tunable SnS_2/SnO_2 nanoheterojunctions (e.g., SnS_2/SnO_2-A, SnS_2/SnO_2-B and SnS_2/SnO_2-C). The photocatalytic properties of the as-synthesized SnS_2/SnO_2 nanoheterojunctions were tested by the reduction of aqueous Cr(VI) under visible-light (λ > 420 nm) irradiation. In addition, the photocatalytic efficiency of SnS_2/SnO_2-B was compared with those of PM-SnS_2/SnO_2 and SnS_2 nanoflakes at different dosages of photocatalysts. The possible formation mechanism of SnS_2/SnO_2 nanoheterojunctions and the reasons accounting for the photocatalytic results were also discussed.

2. Experimental

Tin(IV) chloride pentahydrate ($SnCl_4{\cdot}5H_2O$, ≥99.0%) and thioacetamide (CH_3CSNH_2, ≥99.0%) were of analytical grade, potassium dichromate ($K_2Cr_2O_7$, ≥99.8%) was of guaranteed grade. 50 mg/L $K_2Cr_2O_7$ aqueous solution (pH 5.3) was prepared by dissolving 1500 mg of $K_2Cr_2O_7$ in 30.0 L of deionized water.

2.1. Synthesis

5.0 mmol $SnCl_4{\cdot}5H_2O$ was placed into a 50 mL Teflon-lined stainless steel autoclave, and 40.0 mL of deionized water was added with stirring. After the dissolution of $SnCl_4{\cdot}5H_2O$, 0, 6.0, 7.5, 9.0 or 15.0 mmol CH_3CSNH_2 was added. The above mixture was stirred for 20 min, and a colorless transparent solution was formed. The autoclave was sealed and heated in an electric oven at 190 °C for 6 h, then cooled to room temperature naturally. The resultant precipitate was centrifuged, washed with deionized water, and dried in vacuum at 100 °C for 4 h.

2.2. Characterization

The as-synthesized products were characterized by powder X-ray diffraction (XRD, German Bruker AXS D8 ADVANCE X-ray diffractometer), energy dispersive X-ray spectroscopy (EDX, American Thermo Scientific NORAN System 7 energy dispersive spectrometry system), transmission electron microscopy (TEM, The Netherlands Philips Tecnai-12 electron microscope), high-resolution transmission electron microscopy (HRTEM, American FEI Tecnai G^2 F30 S-TWIN field-emission transmission electron microscopy), X-ray photoelectron spectroscopy (XPS, American Thermo-VG Scientific ESCALAB 250 XPS system, Al K_α radiation and C 1s peak (284.6 eV) reference), N_2 adsorption-desorption isotherms (American Micromeritics Instrument Corporation Tri-Star II 3020 surface area and porosity analyzer), and UV–Vis diffuse reflectance spectra (American Varian Cary 5000 UV–Vis–NIR spectrophotometer). The Cr amount was determined by atomic absorption spectrometry (AAS, German Analytik Jena AG ZEEnit 700 atomic absorption spectrometry, chromium hollow cathode lamp, detection wavelength = 357.9 nm, slit = 0.2 nm and lamp electric current = 5 mA).

2.3. Photocatalytic tests

Photocatalytic properties of the as-synthesized products were tested by the reduction of aqueous Cr(VI) under visible-light (λ > 420 nm) irradiation in custom-made photochemical reactor (Electronic supplementary materials, Fig. S1). Prior to illumination, 300 mL of 50 mg/L $K_2Cr_2O_7$ aqueous solution containing

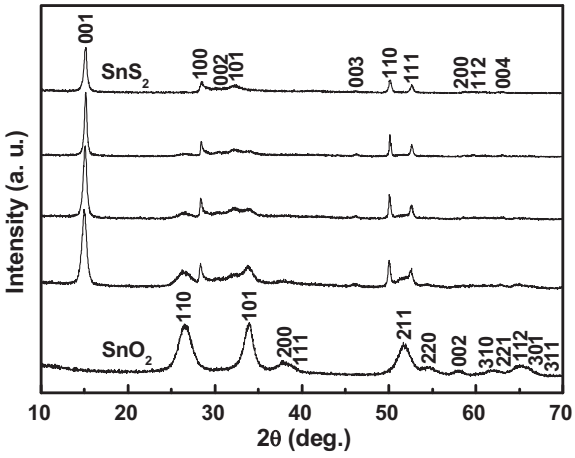

Fig. 1. XRD patterns of the products synthesized using 0, 6.0, 7.5, 9.0 and 15.0 mmol CH_3CSNH_2 from the bottom up.

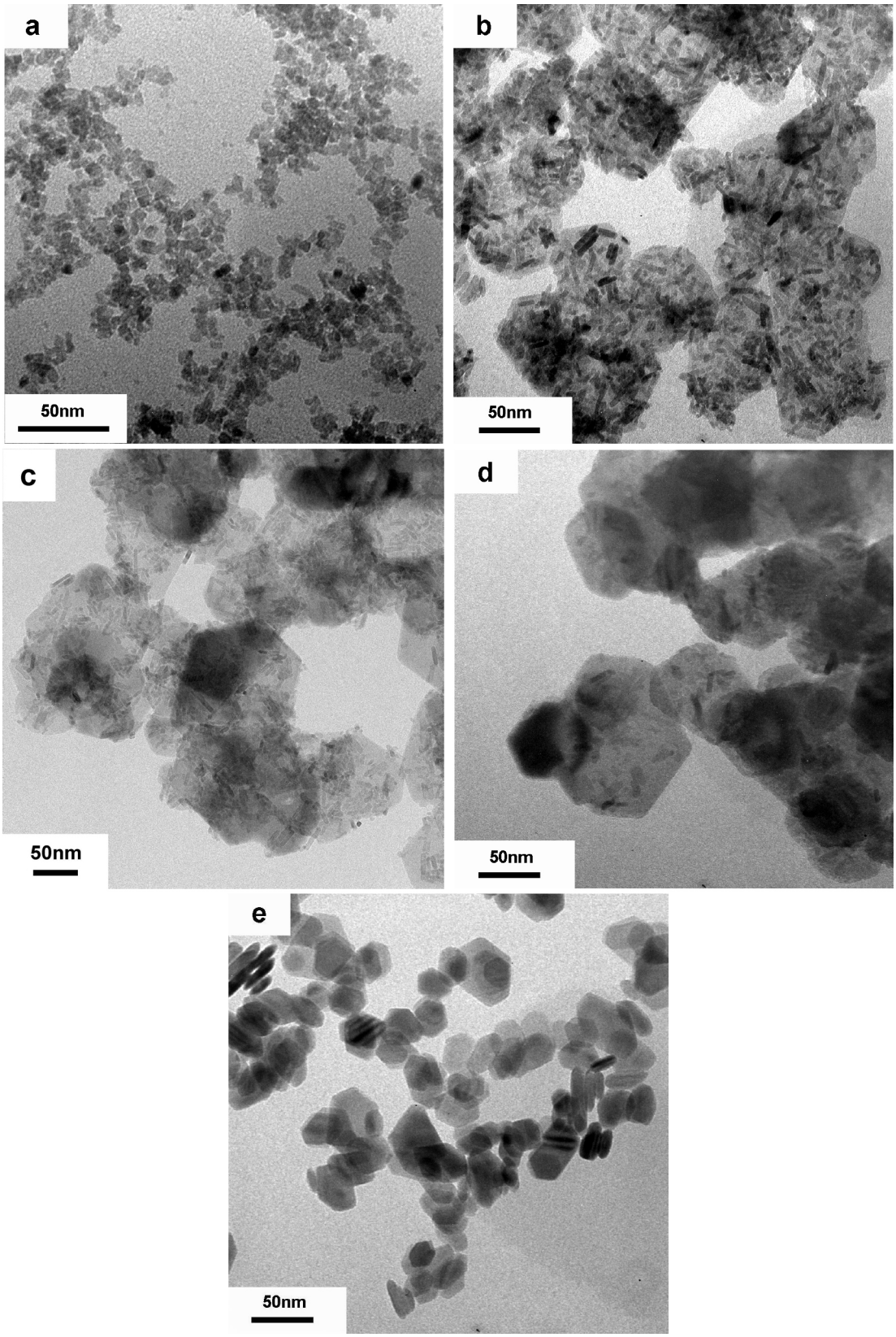

Fig. 2. TEM images of (a) SnO_2, (b) SnS_2/SnO_2-A, (c) SnS_2/SnO_2-B, (d) SnS_2/SnO_2-C and (e) SnS_2.

100–300 mg of photocatalyst was magnetically stirred in dark for 60 min to ensure the adsorption-desorption equilibrium between photocatalyst and Cr(VI) (the results from the dark adsorption experiments and blank experiments were provided in Fig. S2). During illumination, about 3 mL of suspension was taken from the reactor at a scheduled interval and filtered with pore size = 0.22 μm cellulose acetate membrane filter to separate the photocatalyst. The Cr(VI) content in the filtrate was determined colorimetrically using

the standard diphenylcarbazide method with a detection limit of 0.005 mg/L [12].

Each photocatalytic experiment was repeated three times, and the mean value of the three times photocatalytic results was reported here. All the repeated photocatalytic experiments showed good reproducibility, with relative average deviations of <4.5%.

3. Results and discussion

3.1. Compositional and structural characterization

Fig. 1 shows the XRD patterns of the products synthesized using 0, 6.0, 7.5, 9.0 and 15.0 mmol CH_3CSNH_2 from the bottom up. The XRD peaks of the products synthesized using 0 and 15.0 mmol CH_3CSNH_2 can be indexed to pure tetragonal phase SnO_2 (JCPDS card no. 41-1445) and hexagonal phase SnS_2 (JCPDS card no. 89-2358), respectively; whereas those of the products synthesized using 6.0, 7.5 and 9.0 mmol CH_3CSNH_2 indicate the formation of SnS_2 and SnO_2 composites. For the convenience of description, the products synthesized using 0, 6.0, 7.5, 9.0 and 15.0 mmol CH_3CSNH_2 were hereinafter called as "SnO_2", "SnS_2/SnO_2-A", "SnS_2/SnO_2-B", "SnS_2/SnO_2-C" and "SnS_2", respectively. The molar ratios of SnS_2 in SnS_2/SnO_2-A, SnS_2/SnO_2-B and SnS_2/SnO_2-C were determined to be 55%, 70% and 86%, respectively. Evidently, the compositions of the products synthesized by our proposed one-step hydrothermal route can be tuned from SnO_2 to SnS_2/SnO_2 composites to SnS_2, simply by varying the dosage of CH_3CSNH_2.

Fig. 2(a) (b), (c), (d) and (e) shows the TEM images of SnO_2, SnS_2/SnO_2-A, SnS_2/SnO_2-B, SnS_2/SnO_2-C and SnS_2, respectively. As can be seen from Fig. 2(a) and (e), respectively, SnO_2 comprises nanoparticles with diameters of 3–6 nm, whereas SnS_2 comprises nanoflakes with sizes of 22–55 nm. Fig. 2(b)–(d) reveals that SnS_2/SnO_2-A, SnS_2/SnO_2-B and SnS_2/SnO_2-C comprise nanorods/nanoparticles-decorated nanoflakes (further HRTEM characterization reveals that the nanorods/nanoparticles and nanoflakes belong to SnO_2 and SnS_2, respectively). Moreover, all SnO_2 nanorods/nanoparticles are deposited on the surfaces of SnS_2 nanoflakes, and all SnS_2 nanoflakes are decorated with SnO_2 nanorods/nanoparticles, no separated SnO_2 nanorod/nanoparticle and SnS_2 nanoflake can be observed in the TEM images of SnS_2/SnO_2-A, SnS_2/SnO_2-B and SnS_2/SnO_2-C (Fig. 2(b)–(d)), indicating the whole heterojunction structure of SnS_2/SnO_2-A, SnS_2/SnO_2-B and SnS_2/SnO_2-C.

The microstructure of SnS_2/SnO_2-B was further characterized by HRTEM. The HRTEM image in Fig. 3(a) shows that this sample comprises nanoflake decorated with smaller-sized nanorods. The HRTEM image in Fig. 3(b) reveals that the nanoflake displays 0.316 nm fringe intervals, which coincide with the interplanar spacing of (1 0 0) crystal planes of hexagonal phase SnS_2; whereas the smaller-sized nanorods display 0.335 nm fringe intervals, which coincide with the interplanar spacing of (1 1 0) crystal planes of tetragonal phase SnO_2. Thus, the HRTEM results confirm that SnS_2/SnO_2-B has a heterojunction structure.

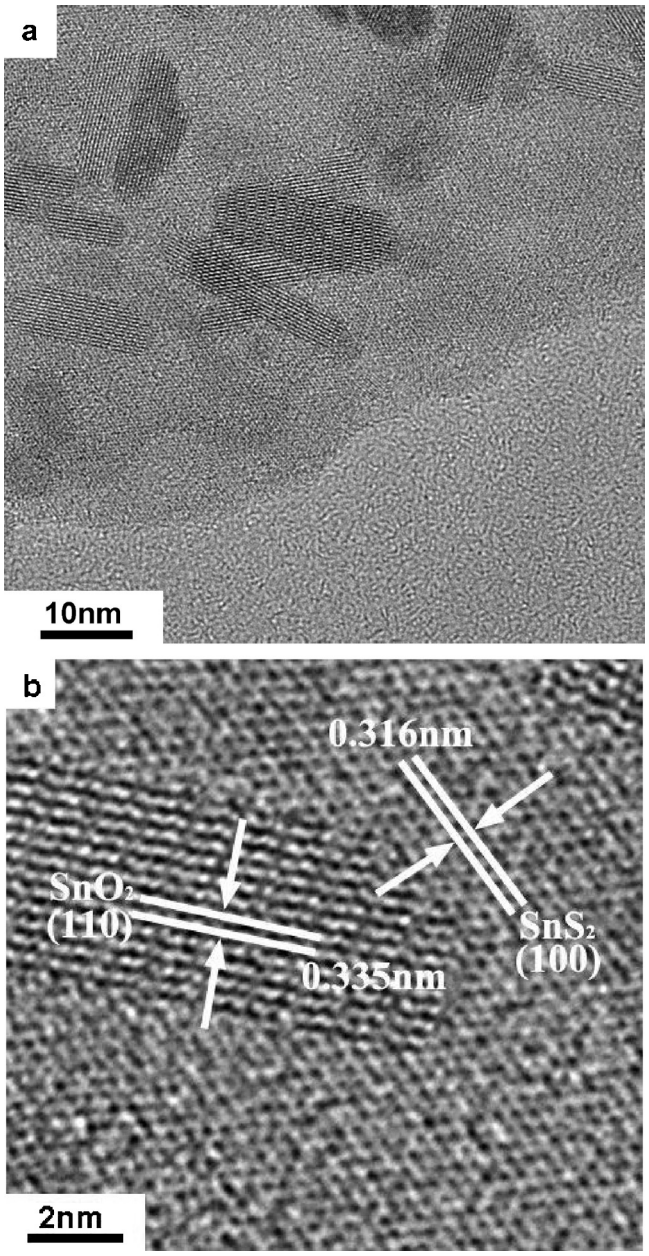

Fig. 3. HRTEM images of SnS_2/SnO_2-B.

3.2. Formation mechanism

In our proposed one-step hydrothermal synthesis of SnS_2/SnO_2 nanoheterojunctions, the source materials used are only $SnCl_4{\cdot}5H_2O$ (whose dosage was fixed at 5.0 mmol), CH_3CSNH_2 and H_2O. $SnCl_4{\cdot}5H_2O$ can dissolve easily in H_2O to release Sn^{4+} (Eq. (1)). CH_3CSNH_2 can hydrolyze in H_2O to yield H_2S (Eq. (2)) [59]. In the presence of suitable amounts (e.g., 6.0–9.0 mmol) of CH_3CSNH_2, Sn^{4+} not only can react with H_2S to form SnS_2 (Eq. (3)), but also can hydrolyze in H_2O to form $Sn(OH)_4$ (Eq. (4)), which can further dehydrate to produce SnO_2 (Eq. (5)) under the 190 °C hydrothermal condition. In the absence of CH_3CSNH_2, only the reactions of Eqs. (1), (4) and (5) take place, resulting in the formation of SnO_2. On the other hand, in the presence of excess (e.g., 15.0 mmol) CH_3CSNH_2, the reactions of Eqs. (1)–(3) become predominant. Furthermore, SnO_2 can be converted to SnS_2 in the presence of excess CH_3CSNH_2 under appropriate hydrothermal conditions (Eq. (6)) [13,29]. Consequently, phase-pure SnS_2 was obtained in the presence of excess (15.0 mmol) CH_3CSNH_2 under the 190 °C hydrothermal condition for 6 h. Thus, SnO_2, SnS_2/SnO_2 nanocomposites with different compositions and SnS_2 can all be synthesized via our proposed one-step hydrothermal route, simply by changing the dosage of CH_3CSNH_2. Besides, the formation of SnS_2/SnO_2 heterojunctions in the current one-pot method may be mainly due to the following two reasons: first, because heterogeneous nucleation requires less energy than homogeneous nucleation [63], SnO_2 tends to nucleate on the surface of SnS_2, and vice versa; second, the high surface energies of nanosized SnO_2

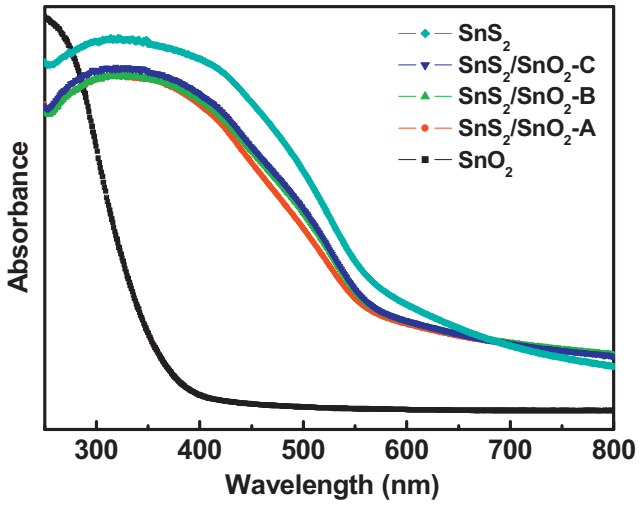

Fig. 4. UV–vis diffuse reflectance spectra of SnO_2, SnS_2/SnO_2-A, SnS_2/SnO_2-B, SnS_2/SnO_2-C and SnS_2 from the bottom up.

and SnS_2 also favor their agglomeration to form heterojunctions [64,65].

$$SnCl_4{\cdot}5H_2O \rightarrow Sn^{4+} + 4Cl^- + 5H_2O \quad (1)$$

$$CH_3CSNH_2 + 2H_2O \rightarrow CH_3COONH_4 + H_2S \quad (2)$$

$$Sn^{4+} + 2H_2S \rightarrow SnS_2 + 4H^+ \quad (3)$$

$$Sn^{4+} + 4H_2O \rightarrow Sn(OH)_4 + 4H^+ \quad (4)$$

$$Sn(OH)_4 \rightarrow SnO_2 + 2H_2O \quad (5)$$

$$SnO_2 + 2H_2S \rightarrow SnS_2 + 2H_2O \quad (6)$$

3.3. BET specific surface areas

The BET specific surface areas of SnO_2, SnS_2/SnO_2-A, SnS_2/SnO_2-B, SnS_2/SnO_2-C and SnS_2 were determined to be 145.5, 90.6, 62.6, 39.8 and 48.1 m^2/g, respectively, based on their N_2 adsorption-desorption isotherms.

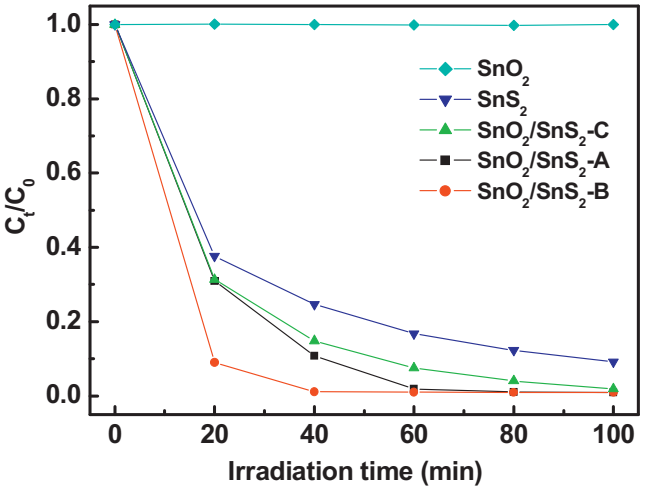

Fig. 5. Photocatalytic activities of SnO_2, SnS_2/SnO_2-A, SnS_2/SnO_2-B, SnS_2/SnO_2-C and SnS_2 in the reduction of aqueous Cr(VI) under visible-light ($\lambda > 420$ nm) irradiation. *Note*: the dosage of photocatalyst is 300 mg; C_0 and C are the concentrations of Cr(VI) aqueous solution when irradiated by visible-light ($\lambda > 420$ nm) light for 0 (i.e., just after the dark adsorption) and t min, respectively.

3.4. Optical properties

Fig. 4 shows the UV–vis diffuse reflectance spectra of SnO_2, SnS_2/SnO_2-A, SnS_2/SnO_2-B, SnS_2/SnO_2-C and SnS_2 in the absorbance mode. As can be seen from Fig. 4, SnO_2 displays no absorption of visible-light; whereas SnS_2/SnO_2-A, SnS_2/SnO_2-B and SnS_2/SnO_2-C, like SnS_2, display prominent photoabsorption ability in the visible region, suggesting that they have the potential to be efficient visible-light-driven photocatalysts. The bandgaps (E_g) of SnO_2, SnS_2/SnO_2-A, SnS_2/SnO_2-B, SnS_2/SnO_2-C and SnS_2 were estimated to be 3.59, 2.27, 2.22, 2.21 and 2.19 eV (Fig. S3), respectively, using the Tauc plot approach [66–69].

3.5. Photocatalytic properties

3.5.1. Photocatalytic activities

Fig. 5 shows the photocatalytic activities of SnO_2, SnS_2/SnO_2-A, SnS_2/SnO_2-B, SnS_2/SnO_2-C and SnS_2 in the reduction of aqueous Cr(VI) under visible-light ($\lambda > 420$ nm) irradiation. As can be seen from Fig. 5, SnO_2 exhibits no visible-light-driven photocatalytic activity, but SnS_2/SnO_2-A, SnS_2/SnO_2-B, SnS_2/SnO_2-C and SnS_2 all exhibit considerably high photocatalytic activities in the reduction of aqueous Cr(VI) under visible-light ($\lambda > 420$ nm) irradiation. The photocatalytic activities of SnS_2/SnO_2-A, SnS_2/SnO_2-B and SnS_2/SnO_2-C are all higher than that of SnS_2. SnS_2/SnO_2-B exhibits the highest photocatalytic activity, which can achieve the reduction of nearly 99% Cr(VI) upon visible-light ($\lambda > 420$ nm) irradiation for 40 min. These photocatalytic results can be rationally explained as follows.

3.5.2. Photocatalytic mechanism

In principle, when semiconductor photocatalysts are irradiated by the light with photon energies greater than or equal to their band gaps, the electrons in their valence bands (VB) can be excited to their conduction bands (CB), simultaneously generating the same number of holes in their VB. The photogenerated electrons (e^-) and holes (h^+) can migrate to the semiconductor surface and participate in the redox reactions with adsorbed species, e.g., in this study, e^- can reduce $Cr_2O_7^{2-}$ to Cr(III); concomitantly, h^+ can oxidize H_2O to O_2 [22–24]. Alternatively, e^- and h^+ can recombine (i.e., the excited electrons revert to VB, dissipating energy as light or heat), losing their photocatalytic activities. The recombination of e^- and h^+ can decrease the overall quantum efficiency and this is the major limitation in semiconductor photocatalysis [24–58].

For SnS_2/SnO_2 nanoheterojunctions upon visible-light ($\lambda > 420$ nm) irradiation, the electrons in the VB of SnS_2 can be excited to its CB with simultaneous generation of an equal amount of h^+ in its VB, while SnO_2 has no visible-light-absorbing ability. Because the VB and CB potentials of SnS_2 are respectively more negative than the VB and CB potentials of SnO_2, e^- can migrate from the CB of SnS_2 to the CB of SnO_2, whereas h^+ still remain in the VB of SnS_2 (Fig. S4). Thus, the separation of e^- and h^+ in SnS_2 can be promoted, and accordingly their recombination is reduced. The more efficient separation of e^- and h^+ can increase their lifetimes and enhance the efficiency of their transfer to the adsorbed substrates [24–58]. In addition, SnO_2 can be activated by the transferred e^-. Hence, it is reasonable that SnS_2/SnO_2-A, SnS_2/SnO_2-B and SnS_2/SnO_2-C can exhibit higher photocatalytic efficiencies than sole SnS_2 under visible-light ($\lambda > 420$ nm) irradiation.

With regard to the difference in the photocatalytic activities of SnS_2/SnO_2-A, SnS_2/SnO_2-B and SnS_2/SnO_2-C, it should be

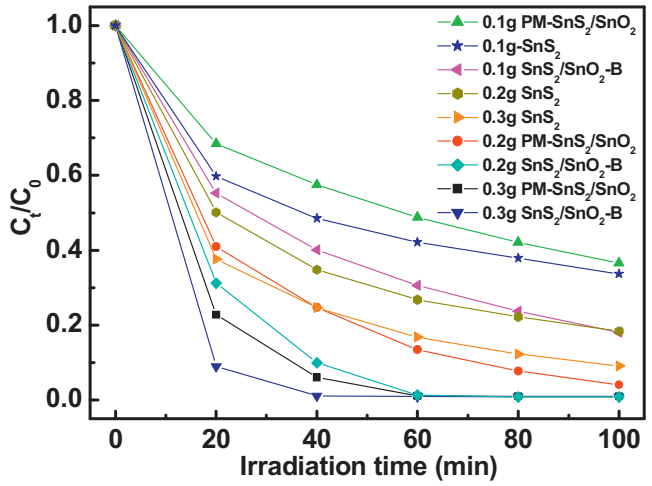

Fig. 6. Comparison of the photocatalytic efficiencies of 100–300 mg of SnS_2, SnS_2/SnO_2-B and PM-SnS_2/SnO_2 in the reduction of aqueous Cr(VI) under visible-light (λ > 420 nm) irradiation.

attributed to the combined action of many factors, such as composition, size, specific surface area and adsorption capacity for Cr(VI), etc. Since all the other influencing factors (e.g., size, specific surface area and adsorption capacity for Cr(VI), etc.) are also dependent on the composition of SnS_2/SnO_2 nanoheterojunctions, it is believed that the composition of SnS_2/SnO_2 nanoheterojunctions should play a dominant role in their photocatalytic activities. SnS_2 possesses relatively high visible-light-driven photocatalytic activity in the reduction of aqueous Cr(VI), whereas SnO_2 has no photocatalytic activity under visible-light (λ > 420 nm) irradiation. More content of SnO_2 means less content of SnS_2 in the SnS_2/SnO_2 nanoheterojunctions, whose dosage was fixed at 300 mg for the photocatalytic experiments in Fig. 5. Less content of the photocatalytically active SnS_2 in SnS_2/SnO_2 nanoheterojunctions can lead to lower photocatalytic efficiency, because the photocatalytic efficiency of SnS_2 is directly proportional to its dosage in the range of 100–300 mg (Fig. 6). Moreover, too much SnO_2 on SnS_2 surface possibly blocks the incident light irradiation on SnS_2 and hinders the contact of SnS_2 with Cr(VI). Therefore, when

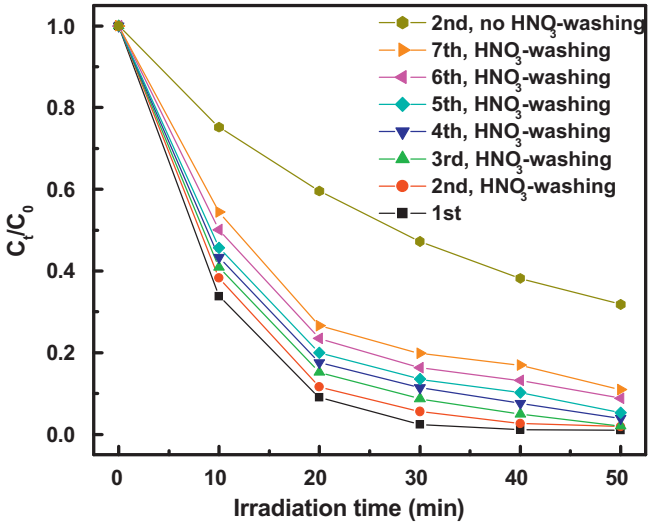

Fig. 7. Photocatalytic performance of SnS_2/SnO_2-B in seven successive cycles of photocatalytic use. *Note*: dosage of photocatalyst = 300 mg; HNO_3-washing = regeneration of the photocatalyst by 1 mol/L HNO_3-washing after use in the previous photocatalytic cycle.

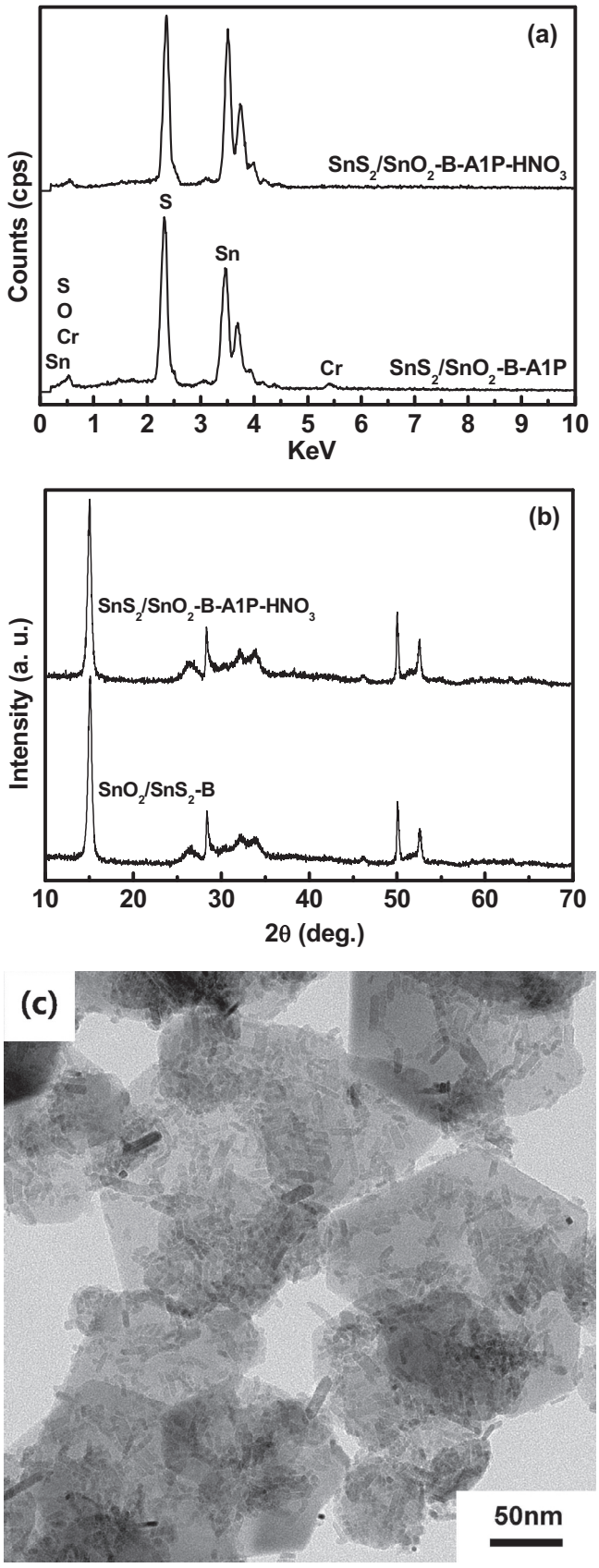

Fig. 8. (a) EDX spectra of SnS_2/SnO_2-B-A1P (SnS_2/SnO_2-B after the first cycle photocatalytic use) and SnS_2/SnO_2-B-A1P-HNO_3 (SnS_2/SnO_2-B-A1P after the 1 mol/L HNO_3-washing treatment); (b) XRD patterns of SnS_2/SnO_2-B and SnS_2/SnO_2-B-A1P-HNO_3; and (c) TEM image of SnS_2/SnO_2-B-A1P-HNO_3.

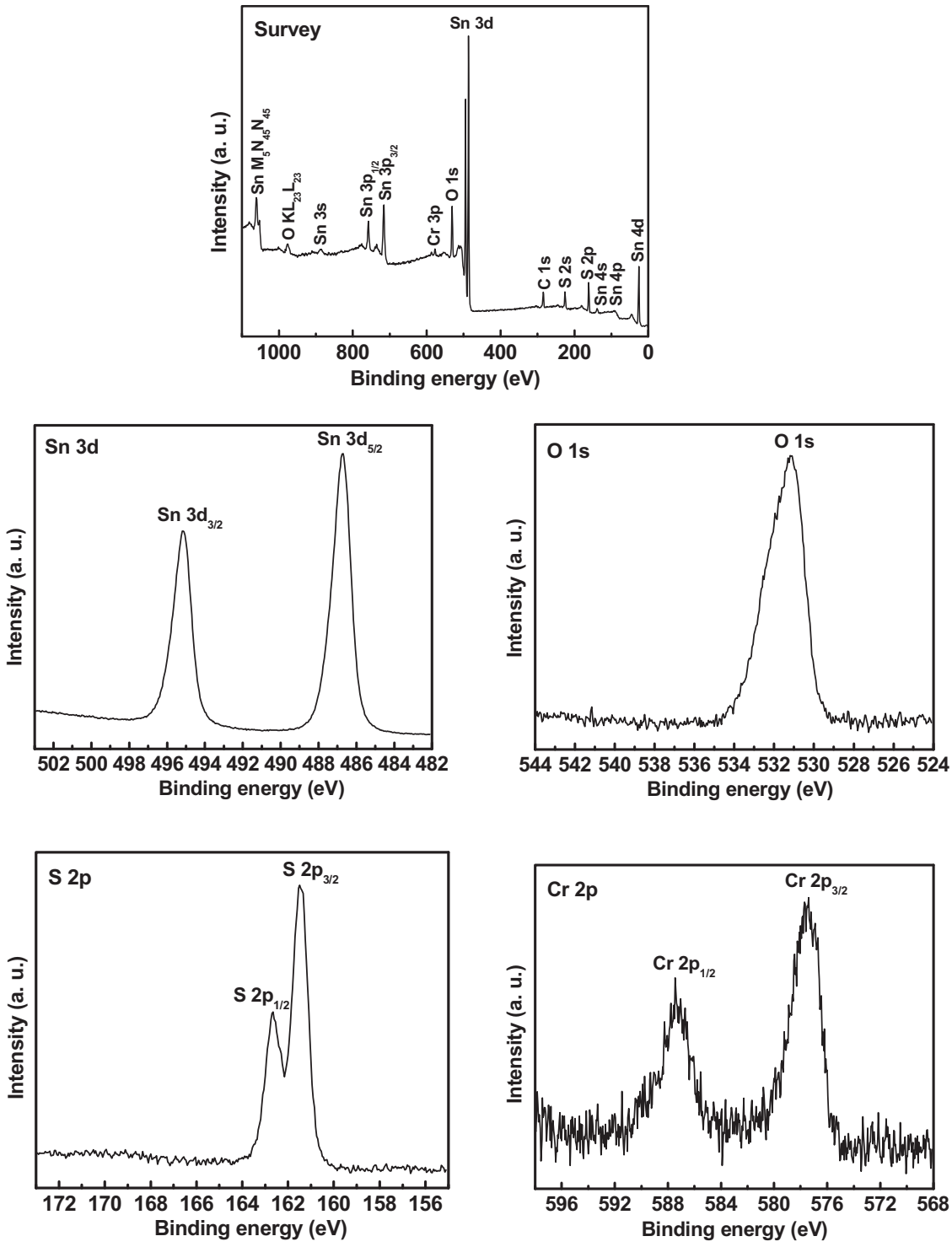

Fig. 9. XPS spectra of SnS_2/SnO_2-B-A7P (SnS_2/SnO_2-B recovered after the seventh cycle photocatalytic use).

SnS_2/SnO_2 nanoheterojunctions have a too high content of SnO_2 (e.g., SnS_2/SnO_2-A), they cannot accomplish the highest photocatalytic efficiency. On the other hand, a too low SnO_2 content in SnS_2/SnO_2 nanoheterojunctions (e.g., SnS_2/SnO_2-C) was also detrimental to maximize the photocatalytic efficiency. This is mainly because when the SnO_2 content in SnS_2/SnO_2 nanoheterojunctions is too low, SnS_2 cannot contact "enough amount" of SnO_2 or the surface of SnS_2 is "insufficiently covered" with SnO_2, which restricts the efficient interfacial electron transfer from SnS_2 to SnO_2. Therefore, there must exist an optimum composition for SnS_2/SnO_2 nanoheterojunctions to achieve the highest photocatalytic efficiency. For the reasons discussed above, SnS_2/SnO_2-B with a suitable content (70 mol%) of SnS_2 exhibits the highest photocatalytic efficiency among SnS_2/SnO_2-A, SnS_2/SnO_2-B and SnS_2/SnO_2-C.

3.5.3. *Influence of heterointerface*

To further show the effect and importance of the heterointerface between the two components of SnS_2/SnO_2 nanocomposite, the photocatalytic efficiencies of 100–300 mg of SnS_2/SnO_2-B,

PM-SnS_2/SnO_2 and SnS_2 in the reduction of aqueous Cr(VI) under visible-light ($\lambda > 420$ nm) irradiation were compared. As can be seen from Fig. 6, 100–300 mg of SnS_2/SnO_2-B invariably exhibits higher photocatalytic efficiencies than the same dosages of PM-SnS_2/SnO_2 and SnS_2. Nevertheless, the comparison results between PM-SnS_2/SnO_2 and SnS_2 depend on their dosages: while 200–300 mg of PM-SnS_2/SnO_2 exhibits higher photocatalytic efficiencies than the same dosages of SnS_2, an inverse conclusion is drawn when their dosage is decreased to 100 mg. The above results manifest definitely that the heterointerface between the two components of SnS_2/SnO_2 nanocomposite plays an important role in their photocatalytic efficiency. When higher concentrations (e.g., 200–300 mg) of PM-SnS_2/SnO_2 are suspended in the Cr(VI) aqueous solution with continuous magnetic stirring, there are still considerable opportunities for the isolated SnS_2 and SnO_2 particles to collide with each other to induce the instantaneous heterointerface. Accordingly, the probability of interfacial electron transfer and electron–hole separation is also relatively high, rendering PM-SnS_2/SnO_2 possess higher photocatalytic efficiency than SnS_2 in the case of larger dosages. Otherwise, when the concentration of PM-SnS_2/SnO_2 is too diluted, the chance of mutual collision between isolated SnS_2 and SnO_2 particles and subsequent interfacial electron transfer become much less, causing 100 mg of PM-SnS_2/SnO_2 to have lower photocatalytic efficiency than the same dosage of SnS_2. Compared with the instantaneous heterointerface created by the random collision between separated SnS_2 and SnO_2 particles of PM-SnS_2/SnO_2, the tight and firm heterojunction structure of SnS_2/SnO_2-B can facilitate interfacial electron transfer and reduce the separation and self-agglomeration of its two components. Therefore, SnS_2/SnO_2-B exhibits the best photocatalytic performance at different dosages of photocatalysts.

3.5.4. Regeneration and reusability of SnS_2/SnO_2-B

After SnS_2/SnO_2-B was used in the photocatalytic reduction of aqueous Cr(VI) under visible-light irradiation for 50 min, it was recovered by centrifugation, washed with deionized water, dried in vacuum at 100 °C for 4 h. Such recovered SnS_2/SnO_2-B (SnS_2/SnO_2-B-A1P) had a green surface color, and its XPS characterization suggested the presence of $Cr(OH)_3$. The composition (i.e., the relative contents of SnS_2 and SnO_2) and structure of SnS_2/SnO_2-B-A1P were almost the same as SnS_2/SnO_2-B. Furthermore, the BET specific surface area (59.1 m^2/g) of SnS_2/SnO_2-B-A1P was also close to that (62.6 m^2/g) of SnS_2/SnO_2-B. However, the photocatalytic activity of SnS_2/SnO_2-B-A1P (Fig. 7(2nd, no HNO_3-washing)) was much lower than that of SnS_2/SnO_2-B (Fig. 7(1st)). This is most likely because that the deposition of $Cr(OH)_3$ on the surface of SnS_2/SnO_2-B-A1P can occupy the photocatalytically active sites, leading to serious deactivation of the photocatalyst [70,71]. In order to remove the $Cr(OH)_3$ deposit from the surface of SnS_2/SnO_2-B-A1P, the washing treatment with 1 mol/L HNO_3 aqueous solution was tried. The results indicated that the 1 mol/L HNO_3-washing treatment can effectively remove $Cr(OH)_3$ from the surface of SnS_2/SnO_2-B-A1P (Fig. 8(a)), without significant change in the composition (i.e., the relative contents of SnS_2 and SnO_2) (Fig. 8(b)), structure (Fig. 8(c)) and BET specific surface area (SnS_2/SnO_2-B-A1P-HNO_3 (SnS_2/SnO_2-B-A1P after the 1 mol/L HNO_3-washing treatment) has a BET specific surface area of 59.6 m^2/g) of the photocatalyst. Meanwhile, most of the lost photocatalytic activity of SnS_2/SnO_2-B-A1P can be regenerated by the 1 mol/L HNO_3-washing treatment (Fig. 7(2nd, HNO_3-washing)). Besides, according to AAS analysis, nearly 98% of the Cr in the initial Cr(VI) aqueous solution can be recovered by the 1 mol/L HNO_3-washing treatment of SnS_2/SnO_2-B-A1P, while the Cr amount left in the aqueous solution after 50 min photocatalytic reactions was negligible, suggesting that almost all the Cr(III) resulting from photocatalytic reduction of Cr(VI) can be adsorbed or precipitated on the photocatalyst. Hence, SnS_2/SnO_2-B has great potential in treating Cr(VI) wastewater by complete removal of Cr species.

Considering the stability of sulfide-based photocatalysts has always been a concern, it is obliged to examine the stability and reusability of SnS_2/SnO_2 nanoheterojunctions in photocatalytic reduction of aqueous Cr(VI). Therefore, in this study, SnS_2/SnO_2-B was recycled for seven times in the same photocatalytic reactions. After each cycle photocatalytic use which lasted 50 min, the photocatalyst was separated from aqueous suspension by centrifugation, washed with 1 mol/L HNO_3 aqueous solution and deionized water, and dried in vacuum at 100 °C for 4 h. Fig. 7 shows the photocatalytic performance of SnS_2/SnO_2-B in seven successive cycles of photocatalytic use. Obviously, the photocatalytic activity of SnS_2/SnO_2-B decreases with increase in the cycle times of photocatalytic use, but such deactivation is moderate. For example, even in the seventh cycle photocatalytic use of SnS_2/SnO_2-B, nearly 89% Cr(VI) can still be reduced upon 50 min visible-light irradiation.

The product recovered after the seventh cycle photocatalytic use of SnS_2/SnO_2-B (SnS_2/SnO_2-B-A7P) was characterized by XPS. The XPS survey spectrum of SnS_2/SnO_2-B-A7P (Fig. 9) reveals the presence of Sn, S, O, Cr and C (the carbon contamination is often ubiquitous in the XPS measurements [72]). The binding energies of Sn $3d_{5/2}$, S $2p_{3/2}$ and O 1s of SnS_2/SnO_2-B-A7P are in turn 486.7, 161.5 and 531.2 eV (Fig. 9), which are consistent with those of Sn^{4+}, S^{2-} and O^{2-} in SnS_2 and SnO_2 [29,31,72]. The binding energy of Cr $2p_{3/2}$ of SnS_2/SnO_2-B-A7P is observed at 577.4 eV (Fig. 9), which corresponds to Cr(III) in $Cr(OH)_3$ [72]. The formation of $Cr(OH)_3$ on the surface of SnS_2/SnO_2-B-A7P can be due to the hydrolysis of Cr(III), which is generated from the photocatalytic reduction of adsorbed Cr(VI) [73].

4. Conclusions

Composition-tunable synthesis of SnS_2/SnO_2 nanoheterojunctions was achieved by our proposed one-step hydrothermal method. This method is simple and using only common and inexpensive reactants ($SnCl_4{\cdot}5H_2O$, CH_3CSNH_2 and H_2O), thus it is viable for large-scale production of SnS_2/SnO_2 nanoheterojunctions.

Through the photocatalytic experiments using aqueous Cr(VI) as a probe pollutant under visible-light ($\lambda > 420$ nm) irradiation, the following results were obtained: (i) the photocatalytic activities of SnS_2/SnO_2 nanoheterojunctions depended on their compositions, and SnS_2/SnO_2-B displayed the highest photocatalytic activity; (ii) 100–300 mg of SnS_2/SnO_2-B always exhibited higher photocatalytic efficiencies than the same dosages of PM-SnS_2/SnO_2 and SnS_2; (iii) SnS_2/SnO_2-B demonstrated good reusability in photocatalytic reduction of aqueous Cr(VI), with regeneration by 1 mol/L HNO_3-washing after each cycle of photocatalytic use; and (iv) Cr(VI) was reduced to Cr(III). These results suggest that SnS_2/SnO_2-B is a promising visible-light-activated photocatalyst in efficient utilization of solar energy for Cr(VI) wastewater treatment.

Acknowledgements

Dr. Dionysiou acknowledges support from the National Science Foundation (US-Ireland collaborative research CBET (1033317) for his involvement on this project. This work was partially funded by the Cyprus Research Promotion Foundation through Desmi 2009-2010 which is co-funded by the Republic of Cyprus and the European Regional Development Fund of the EU under contract number NEA IPODOMI/STRATH/0308/09. This is also a project

funded by the Priority Academic Program Development of Jiangsu Higher Education Institutions, China Scholarship Council (CSC) Scholarships (2011832350), and the Science & Technology Innovation Fund of Yangzhou University (2012CXJ017). Thanks to The Testing Center of Yangzhou University for the characterization data.

Appendix A. Supplementary data

Supplementary data associated with this article can be found, in the online version, at http://dx.doi.org/10.1016/j.apcatb.2013.08.006.

References

[1] L. Yang, Y. Xiao, S. Liu, Y. Li, Q. Cai, S. Luo, Appl. Catal. B 94 (2010) 142–149.
[2] H. Chen, Y. Shao, Z. Xu, H. Wan, Y. Wan, S. Zheng, Appl. Catal. B 105 (2011) 255–262.
[3] R. Brahimi, Y. Bessekhouad, N. Nasrallah, M. Trari, J. Hazard. Mater. 219–220 (2012) 19–25.
[4] G. Chen, M. Sun, Q. Wei, Z. Ma, B. Du, Appl. Catal. B 125 (2012) 282–287.
[5] Y.C. Zhang, M. Yang, G. Zhang, D.D. Dionysiou, Appl. Catal. B 142–143 (2013) 249–258.
[6] G. Qin, C. Wang, X. Tong, S. Xue, Appl. Catal. B 142–143 (2013) 142–148.
[7] C. Alanis, R. Natividad, C. Barrera-Diaz, V. Martínez-Miranda, J. Prince, J.S. Valente, Appl. Catal. B 140–141 (2013) 546–551.
[8] P.S. Suchithra, C.P. Shadiya, A.P. Mohamed, P. Velusamy, S. Ananthakumar, Appl. Catal. B 130–131 (2013) 44–53.
[9] H.T. Hsu, S.S. Chen, Y.S. Chen, Sep. Purif. Technol. 80 (2011) 663–669.
[10] S. Luo, Y. Xiao, L. Yang, C. Liu, F. Su, Y. Li, Sep. Purif. Technol. 79 (2011) 85–91.
[11] N. Wang, L. Zhu, K. Deng, Y. She, Y. Yu, H. Tang, Appl. Catal. B 95 (2010) 400–407.
[12] T.X. Wang, S.H. Xu, F.X. Yang, Mater. Lett. 83 (2012) 46–48.
[13] J. Wang, X. Li, X. Li, J. Zhu, H. Li, Nanoscale 5 (2013) 1876–1881.
[14] A.E. Giannakas, E. Seristatidou, Y. Deligiannakis, I. Konstantinou, Appl. Catal. B 132–133 (2013) 460–468.
[15] A.E. Giannakas, M. Antonopoulou, Y. Deligiannakis, I. Konstantinou, Appl. Catal. B 140–141 (2013) 636–645.
[16] Y. Zhang, Z. Chen, S. Liu, Y.J. Xu, Appl. Catal. B 140–141 (2013) 598–607.
[17] S.K. Choi, H.S. Yang, J.H. Kim, H. Park, Appl. Catal. B 121–122 (2012) 206–213.
[18] S. Liu, N. Zhang, Z.R. Tang, Y.J. Xu, ACS Appl. Mater. Interfaces 4 (2012) 6378–6385.
[19] A. Kleiman, A. Márquez, M.L. Vera, J.M. Meichtry, M.I. Litter, Appl. Catal. B 101 (2011) 676–681.
[20] G. Kim, W. Choi, Appl. Catal. B 100 (2010) 77–83.
[21] H. Ma, J. Shen, M. Shi, X. Lu, Z. Li, Y. Long, Appl. Catal. B 121–122 (2012) 198–205.
[22] X. An, J.C. Yu, F. Wang, C. Li, Y. Li, Appl. Catal. B 129 (2013) 80–88.
[23] L. Wang, X. Li, W. Teng, Q. Zhao, Y. Shi, R. Yue, Y. Chen, J. Hazard. Mater. 244–245 (2013) 681–688.
[24] Y.C. Zhang, J. Li, H.Y. Xu, Appl. Catal. B 123–124 (2012) 18–26.
[25] S. Ding, X. Yin, X. Lü, Y. Wang, F. Huang, D. Wan, ACS Appl. Mater. Interfaces 4 (2012) 306–311.
[26] C. Yang, W. Wang, Z. Shan, F. Huang, J. Solid State Chem. 182 (2009) 807–812.
[27] J. Li, T. Wang, X. Du, Sep. Purif. Technol. 101 (2012) 11–17.
[28] H. Huang, D. Li, Q. Lin, W. Zhang, Y. Shao, Y. Chen, M. Sun, X. Fu, Environ. Sci. Technol. 43 (2009) 4164–4168.
[29] Y.C. Zhang, Z.N. Du, K.W. Li, M. Zhang, D.D. Dionysiou, ACS Appl. Mater. Interfaces 3 (2011) 1528–1537.
[30] Y.C. Zhang, Z.N. Du, M. Zhang, Mater. Lett. 65 (2011) 2891–2894.
[31] X. Zhou, T. Zhou, J. Hu, J. Li, CrystEngComm 14 (2012) 5627–5633.
[32] Y.P. Yuan, S.W. Cao, Y.S. Liao, L.S. Yin, C. Xue, Appl. Catal. B 140–141 (2013) 164–168.
[33] J. Cao, B. Luo, H. Lin, B. Xu, S. Chen, Appl. Catal. B 111–112 (2012) 288–296.
[34] T. Li, L. Zhao, Y. He, J. Cai, M. Luo, J. Lin, Appl. Catal. B 129 (2013) 255–263.
[35] H. Xu, J. Yan, Y. Xu, Y. Song, H. Li, J. Xia, Appl. Catal. B 129 (2013) 182–193.
[36] L. Ge, J. Liu, Appl. Catal. B 105 (2011) 289–297.
[37] Z. Zhang, W. Wang, L. Wang, S. Sun, ACS Appl. Mater. Interfaces 4 (2012) 593–597.
[38] K. Sridharan, E. Jang, T.J. Park, Appl. Catal. B 142–143 (2013) 718–728.
[39] J. Hou, C. Yang, Z. Wang, Q. Ji, Y. Li, G. Huang, S. Jiao, Appl. Catal. B 142–143 (2013) 579–589.
[40] N. Wetchakun, S. Chaiwichain, B. Inceesungvorn, K. Pingmuang, S. Phanichphant, A.I. Minett, ACS Appl. Mater. Interfaces 4 (2012) 3718–3723.
[41] Y. Shi, H. Li, L. Wang, W. Shen, H. Chen, ACS Appl. Mater. Interfaces 4 (2012) 4800–4806.
[42] F.X. Xiao, ACS Appl. Mater. Interfaces 4 (2012) 7055–7063.
[43] H. Fan, H. Li, B. Liu, Y. Lu, T. Xie, D. Wang, ACS Appl. Mater. Interfaces 4 (2012) 4853–4857.
[44] V. Etacheri, G. Michlits, M.K. Seery, S.J. Hinder, S.C. Pillai, ACS Appl. Mater. Interfaces 5 (2013) 1663–1672.
[45] M. Pelaez, N.T. Nolan, S.C. Pillai, M.K. Seery, P. Falaras, A.G. Kontos, Appl. Catal. B 125 (2012) 331–349.
[46] W. Li, D. Li, S. Meng, W. Chen, X. Fu, Y. Shao, Environ. Sci. Technol. 45 (2011) 2987–2993.
[47] D. He, L. Wang, D. Xu, J. Zhai, D. Wang, T. Xie, ACS Appl. Mater. Interfaces 3 (2011) 3167–3171.
[48] T.J. Athauda, J.G. Neff, ACS Appl. Mater. Interfaces 4 (2012) 6917–6926.
[49] Y.F. Lin, Y.J. Hsu, Appl. Catal. B 130–131 (2013) 93–98.
[50] S. Shenawi-Khalil, V. Uvarov, S. Fronton, I. Popov, Y. Sasson, Appl. Catal. B 117–118 (2012) 148–155.
[51] W. Zhao, Y. Wang, Y. Yang, J. Tang, Y. Yang, Appl. Catal. B 115–116 (2012) 90–99.
[52] J. Guo, S. Ouyang, P. Li, Y. Zhang, T. Kako, J. Ye, Appl. Catal. B 134–135 (2013) 286–292.
[53] Y.S. Xu, W.D. Zhang, Appl. Catal. B 140–141 (2013) 306–316.
[54] Y. Huang, Y. Wei, J. Wu, C. Guo, M. Wang, S. Yin, T. Sato, Appl. Catal. B 123–124 (2012) 9–17.
[55] W. Wang, X. Huang, S. Wu, Y. Zhou, L. Wang, H. Shi, Appl. Catal. B 134–135 (2013) 293–301.
[56] Y. Hu, D. Li, Y. Zheng, W. Chen, Y. He, Y. Shao, X. Fu, Appl. Catal. B 104 (2011) 30–36.
[57] J. Xu, W. Wang, S. Sun, L. Wang, Appl. Catal. B 111–112 (2012) 126–132.
[58] D. Sarkar, C.K. Ghosh, S. Mukherjee, K.K. Chattopadhyay, ACS Appl. Mater. Interfaces 5 (2013) 331–337.
[59] Y.C. Zhang, Z.N. Du, K.W. Li, M. Zhang, Sep. Purif. Technol. 81 (2011) 101–107.
[60] R. Lucena, F. Fresno, J.C. Conesa, Appl. Catal. A 415–416 (2012) 111–117.
[61] X. Li, J. Zhu, H. Li, Appl. Catal. B 123–124 (2012) 174–181.
[62] Y.C. Zhang, Z.N. Du, S.Y. Li, M. Zhang, Appl. Catal. B 95 (2010) 153–159.
[63] P.G. Vekilov, Crystal Growth Des. 10 (2010) 5007–5019.
[64] M. Shim, H. McDaniel, Curr. Opin. Solid State Mater. Sci. 14 (2010) 83–94.
[65] L. Carbone, P.D. Cozzoli, Nano Today 5 (2010) 449–493.
[66] T. Warang, N. Patel, R. Fernandes, N. Bazzanella, A. Miotello, Appl. Catal. B 132–133 (2013) 204–211.
[67] X. Xu, R. Lu, X. Zhao, Y. Zhu, S. Xu, F. Zhang, Appl. Catal. B 125 (2012) 11–20.
[68] Y. Liang, P. Liu, H.B. Li, G.W. Yang, Crystal Growth Des. 12 (2012) 4487–4493.
[69] X. Liang, L. Xing, J. Xiang, F. Zhang, J. Jiao, L. Cui, Crystal Growth Des. 12 (2012) 1173–1179.
[70] A. Idris, N. Hassan, R. Rashid, A.F. Ngomsik, J. Hazard. Mater. 186 (2011) 629–635.
[71] S. Tuprakay, W. Liengcharernsit, J. Hazard. Mater. 124 (2005) 53–58.
[72] J.F. Moulder, W.F. Stickle, P.E. Sobol, K.D. Bomben, in: J. Chastain (Ed.), Handbook of X-ray Photoelectron Spectroscopy, Perkin-Elmer Corp, Eden Prairie, 1992.
[73] Y.C. Zhang, J. Li, M. Zhang, D.D. Dionysiou, Environ. Sci. Technol. 45 (2011) 9324–9331.